

# Helium enrichment in intermediate-age Magellanic Clouds clusters: towards an ubiquity of multiple stellar populations?

W. Chantereau,<sup>1</sup>★ M. Salaris,<sup>1</sup> N. Bastian,<sup>1</sup> S. Martocchia<sup>2,1</sup>

<sup>1</sup>*Astrophysics Research Institute, Liverpool John Moores University, 146 Brownlow Hill, Liverpool L3 5RF, UK*

<sup>2</sup>*European Southern Observatory, Karl-Schwarzschild-Straße 2, D-85748 Garching bei München, Germany*

Accepted XXX. Received YYY; in original form ZZZ

## ABSTRACT

Intermediate-age star clusters in the Magellanic Clouds harbour signatures of the multiple stellar populations long thought to be restricted to old globular clusters. We compare synthetic horizontal branch models with *Hubble Space Telescope* photometry of clusters in the Magellanic Clouds, with age between  $\sim 2$  and  $\sim 10$  Gyr, namely NGC 121, Lindsay 1, NGC 339, NGC 416, Lindsay 38, Lindsay 113, Hodge 6 and NGC 1978. We find a clear signature of initial helium abundance spreads ( $\Delta Y$ ) in four out of these eight clusters (NGC 121, Lindsay 1, NGC 339, NGC 416) and we quantify the value of  $\Delta Y$ . For two clusters (Lindsay 38, Lindsay 113) we can only determine an upper limit for  $\Delta Y$ , whilst for the two youngest clusters in our sample (Hodge 6 and NGC 1978) no conclusion about the existence of an initial He spread can be reached. Our  $\Delta Y$  estimates are consistent with the correlation between maximum He abundance spread and mass of the host cluster found in Galactic globular clusters. This result strengthens the emerging view that the formation of multiple stellar populations is a standard process in massive star clusters, not limited to a high redshift environment.

**Key words:** stars: abundances – stars: chemically peculiar – stars: horizontal branch – Hertzsprung-Russell and colour-magnitude diagrams – galaxies: individual: SMC – galaxies: individual: LMC

## 1 INTRODUCTION

The multiple stellar populations (MPs) present in individual globular clusters (GCs) are characterised by star-to-star abundance anti-correlations of light elements (C-N, O-Na and Mg-Al to a certain extent) together with spreads of initial He abundances (e.g. Milone et al. 2018; Bastian & Lardo 2018). It has been recently shown that massive intermediate-age clusters in the Magellanic Clouds (MCs) –with ages down to  $\sim 2$  Gyr– also display light element abundance patterns like GCs (e.g. Hollyhead et al. 2017; Niederhofer et al. 2017a,b). On the other hand, clusters younger than  $\sim 2$  Gyr seem to lack detectable MPs, suggesting that age (or stellar mass) play a major factor in the onset of this phenomenon in massive stellar clusters (Martocchia et al. 2018a).

An important question to be addressed is the following: Do the MCs massive clusters older than  $\sim 2$  Gyr also display He abundance spreads, like Galactic GCs? If this is the case, these intermediate-age clusters are the counterparts of Galactic GCs in terms of MPs, thus suggesting that the MP formation is not restricted to high redshift environments. This, in turn, implies that young stellar clusters can also be used to constrain the MP formation process.

In a very recent paper, Lagioia et al. (2019) determined the presence of He abundance spread in four SMC massive clus-

ters, employing photometry of red giant branch (RGB) stars. They found small helium abundance spreads in NGC 121, NGC 339 and NGC 416, while no spread was found for Lindsay 1.

Here, we will investigate the presence of a He abundance spread in a sample of MC clusters by modelling the morphology of their Red Clump (RC) and red horizontal branch (HB) stars in the colour-magnitude-diagram (CMD) using synthetic HB (and RC) models. As is well known, the CMD morphology of the He-burning phase is very sensitive to the initial He abundance of the parent populations, and indeed synthetic HB models have been employed to determine He abundance spreads in Milky Way GCs such as NGC 104 (Gratton et al. 2013), NGC 2419 (di Criscienzo et al. 2011; Di Criscienzo et al. 2015), NGC 2808 (Dalessandro et al. 2011), NGC 5272 (Dalessandro et al. 2013), NGC 5904 (Gratton et al. 2013), NGC 6388 (Busso et al. 2007), and NGC 6441 (Busso et al. 2007; Caloi & D’Antona 2007).

The massive, intermediate-age clusters investigated in this study are Lindsay 1, NGC 121, NGC 339, NGC 416, in common with Lagioia et al. (2019), plus Hodge 6, Lindsay 38, Lindsay 113 and NGC 1978. They are all younger than the average Milky Way GC, with ages ranging between  $\sim 2$  Gyr and  $\sim 10$  Gyr. Additionally, all clusters have had MP signatures detected within them either photometrically or spectroscopically, except Lindsay 38 and Lindsay 113 that are currently being investigated (Martocchia et al. 2019, in preparation).

★ E-mail: w.chantereau@ljmu.ac.uk

Our study expands the sample of clusters in the MCs investigated for the presence of initial He abundance spreads. Also, our method is complementary to the technique employed by Lagioia et al. (2019). These latter authors model several colour differences –sensitive to He, C, N, O abundance spreads– between fiducial sequences that trace the RGB of the main populations of each cluster (for one cluster they also determine the He spread from the RGB bump, whose brightness is also sensitive to the initial He abundance). As such, their method tends to measure differences of mean He abundances between cluster subpopulations. Our HB modelling aims at reproducing the full colour and magnitude range of the observed HBs, and should estimate the maximum He spread amongst stars in individual clusters.

The paper is organised as follows. Sect. 2 that describes both stellar evolution models and observations employed in this paper. Section 3 describes briefly the synthetic HB models, how they can reveal the presence of initial  $Y$  variations, and the fitting procedure to observational data. In Sect. 4 we investigate the presence of  $Y$  variations in individual clusters in our sample, and in Sect. 5 we finally discuss and summarise our results.

## 2 STELLAR MODELS AND OBSERVATIONS

We employ non-rotating stellar evolution models and tracks computed with the code STAREVOL (e.g. Lagarde et al. 2012). Our calculations do not include atomic diffusion<sup>1</sup>. For each assumed cluster metallicity and age, we have computed models –from the zero age main sequence to the end of the HB, following the evolution through the He-flash– with various values of the initial Helium mass fraction ( $Y$ ), choosing appropriate initial main sequence masses to reach the cluster age at the beginning of the He-burning phase. Our calculations do not include the early-asymptotic giant branch phase following the exhaustion of central He. The  $Y$  values range from the value expected from Galactic chemical evolution ( $\Delta Y/\Delta Z \sim 1.57$ ) to the maximum values given in Table 1, that vary from cluster to cluster.

As for the metal distribution of our models, we assume a scaled solar distribution (Asplund et al. 2009, with an  $\alpha$ -enhancement for the case of NGC 104 and NGC 121, see next section). Also, the He-enhanced models (that in principle should have metal distributions with altered C, N, O, Na, Mg, Al abundances) are calculated for the same scaled solar (or  $\alpha$ -enhanced) metal mixture, given that stellar evolution is not affected by these abundance variations if the sum of the C+N+O abundance is kept constant at fixed metallicity (as generally observed, within the errors, in Galactic GCs, see e.g. Yong et al. 2015). In addition, we work on CMDs in the ACS and WFC3 F475W, F555W, and F814W photometric bands, that are insensitive to variations of these light elements (see e.g., Salaris et al. 2006; Sbordone et al. 2011).

Mass-loss during the red giant branch (RGB) evolution is accounted for by employing the Reimers formula (Reimers 1975):

$$\dot{M} = 4 \times 10^{-13} \eta_R \frac{LR}{M} M_{\odot} yr^{-1}$$

where  $L$ ,  $M$  and  $R$  are the model luminosity, mass and radius in solar units. For each metallicity and  $Y$  abundances we have calculated tracks for various values of  $\eta_R$ .

<sup>1</sup> All observed HBs and RCs investigated here are cool enough ( $T_{\text{eff}} \lesssim 10^4$  K) to avoid strong effects of atomic diffusion (Hui-Bon-Hoa et al. 2000; Michaud et al. 2011).

Bolometric corrections to the ACS and WFC3 filters are obtained by interpolation amongst the tables from the MIST database (Choi et al. 2016)<sup>2</sup>.

Clusters' photometries are taken from the *Hubble Space Telescope* survey presented in Niederhofer et al. (2017a,b); Martocchia et al. (2018a) and Martocchia et al. (*in prep.*). In this study we use the ACS F555W and F814W optical filters, except for Hodge 6, for which we use WFC3 photometry in the F475W and F814W filters. The cluster CMDs are shown in Fig. 1, and the relevant cluster properties are listed in Table 1.

Niederhofer et al. (2017a,b); Martocchia et al. (2018a) and Martocchia et al. (*in prep.*) investigated these clusters for differential reddening and only NGC 416 is affected (we refer to these works for more details). Thus we use the data corrected for differential reddening for this cluster.

## 3 SYNTHETIC HORIZONTAL BRANCH MODELLING

To determine the theoretical cluster HB (or RC) location and morphology in the CMD we need to fix a number of parameters, namely the cluster age, metallicity, initial He distribution, RGB mass loss efficiency ( $\eta_R$ , that determines the actual mass of the synthetic HB stars for a given cluster age and initial chemical composition). For each cluster, we fix age and metallicity to the values estimated in previous studies, as reported in Table 1. Notice that variations of the age around the values in Table 1 will change the derived value of  $\eta_R$  (because of a different HB progenitor mass) but not the overall results about the presence (or absence) of a He abundance spread in individual clusters. Also, the minimum value of  $Y$  (that we denote as the He abundance of the He-normal population) is fixed to the value given by  $Y = Y_0 + \Delta Y/\Delta Z \times Z$  where  $Z$  is the heavy element mass fraction. The primordial helium mass fraction  $Y_0$  chosen is equal to 0.2479 (Coc et al. 2004).

The free parameters that are left to be determined by fitting synthetic HBs to observed CMDs are the minimum and eventually maximum value of  $\eta_R$  (if the observed HB is matched with a spread of mass loss instead of  $Y$ ), and the maximum value of  $Y$  (if a range of  $Y$  is required). For simplicity, we assume a uniform probability distribution for  $\eta_R$  and  $Y$ , between the minimum and maximum values. We interpolate in  $Y$  and  $\eta_R$  amongst our model grid to determine the HB track of our synthetic star for a given  $\eta_R$  and  $Y$ . We then extract a random age with uniform probability between the zero age HB and the exhaustion of central He points, to fix the position of the synthetic stars in the CMD<sup>3</sup>. Magnitudes and colours of the synthetic stars are then perturbed by random Gaussian photometric errors, with  $1\sigma$  values taken from the mean photometric errors of the observations. We also checked these errors by comparing with the RGB width. We verticalised the RGB to determine the standard deviation of the  $\delta(\text{colour})$  distribution of RGB stars at the HB magnitude level. The standard deviation then derived is similar to the photometric errors of the observations, in addition this standard deviation can be considered as an upper limit since the He spread also affects the RGB width. Thus we are confident with these photometric errors. For each cluster we create the same number of synthetic stars as the one observed in a box delimiting the HB region of each cluster.

The procedure adopted to match the observed HB of a given

<sup>2</sup> [http://waps.cfa.harvard.edu/MIST/model\\_grids.html](http://waps.cfa.harvard.edu/MIST/model_grids.html)

<sup>3</sup> The underlying standard assumptions is that stars are fed to the HB at a constant rate.

ID	[Fe/H]	Age (Gyr)	Ref.	Cluster		$(m - M)_V$	$E(B - V)$	Ref.	minimum $Y$ models		maximum $Y$ models	
				Mass ( $M_\odot$ )	Ref.				$Y_{\text{ini}}$	$M_{\text{ini}} (M_\odot)$	$Y_{\text{ini}}$	$M_{\text{ini}} (M_\odot)$
NGC 104	-0.72	12.0	M15	$7.79 \times 10^5$	B18	13.37	0.04	H96	0.251	0.905	0.291	0.84
NGC 121	-1.30	10.5	G8a,N17	$5.83 \times 10^5$	G11	19.00	0.03	G8a,N17a	0.248	0.89	0.288	0.83
Lindsay 1	-1.14	$7.5 \pm 0.5$	G8b	$1.74 \times 10^5$	G11	18.78	0.02	G8b	0.249	0.97	0.279	0.92
NGC 339	-1.12	$6 \pm 0.5$	G8b	$2.88 \times 10^5$	G11	18.80	0.02	G8b	0.250	1.04	0.290	0.97
NGC 416	-1.00	$6 \pm 0.5$	G8b	$2.32 \times 10^5$	G11	18.90	0.08	G8b	0.250	1.045	0.330	0.905
Lindsay 38	-1.50	$6 \pm 0.5$	M19	$3.35 \times 10^4$	G11	19.10	0.02	M19	0.249	1.02	0.269	0.985
Lindsay 113	-1.40	$4.5 \pm 0.5$	M19	$\sim 2.3 \times 10^4$	C10	18.85	0.02	M19	0.249	1.11	0.269	1.07
Hodge 6	-0.40	$2.25 \pm 0.05$	P14,G14	$5.5 \times 10^4$	G14	18.77	0.09	P14	0.258	1.53	0.318	1.37
NGC 1978	-0.35	$1.9 \pm 0.1$	M07	$2 - 4 \times 10^5$	W97	18.71	0.05	M18b	0.258	1.60	0.288	1.51

**Table 1.** Adopted parameters for the clusters we investigate in this study. Note that the minimum and maximum  $Y$  models displayed in this table are the models of our grid we use to interpolate in between to create the synthetic HB models (cf text). References: (M15) McDonald & Zijlstra (2015); (B18) Baumgardt & Hilker (2018); (H96) Harris (1996), 2010 edition; (G8a) Glatt et al. (2008a); (N17) Niederhofer et al. (2017a); (G11) Glatt et al. (2011); (G8b) Glatt et al. (2008b); (M19) Martocchia et al. (in prep.); (C10) Computed from the absolute magnitude in the V band (-5.29, Carretta et al. 2010) and adopting a mass-to-light ratio of  $\sim 2$  (Baumgardt & Hilker 2018); (P14) Piatti et al. (2014); (G14) Goudfrooij et al. (2014); (M07) Mucciarelli et al. (2007); (W97) Westerlund (1997), (M18b) Martocchia et al. (2018b).

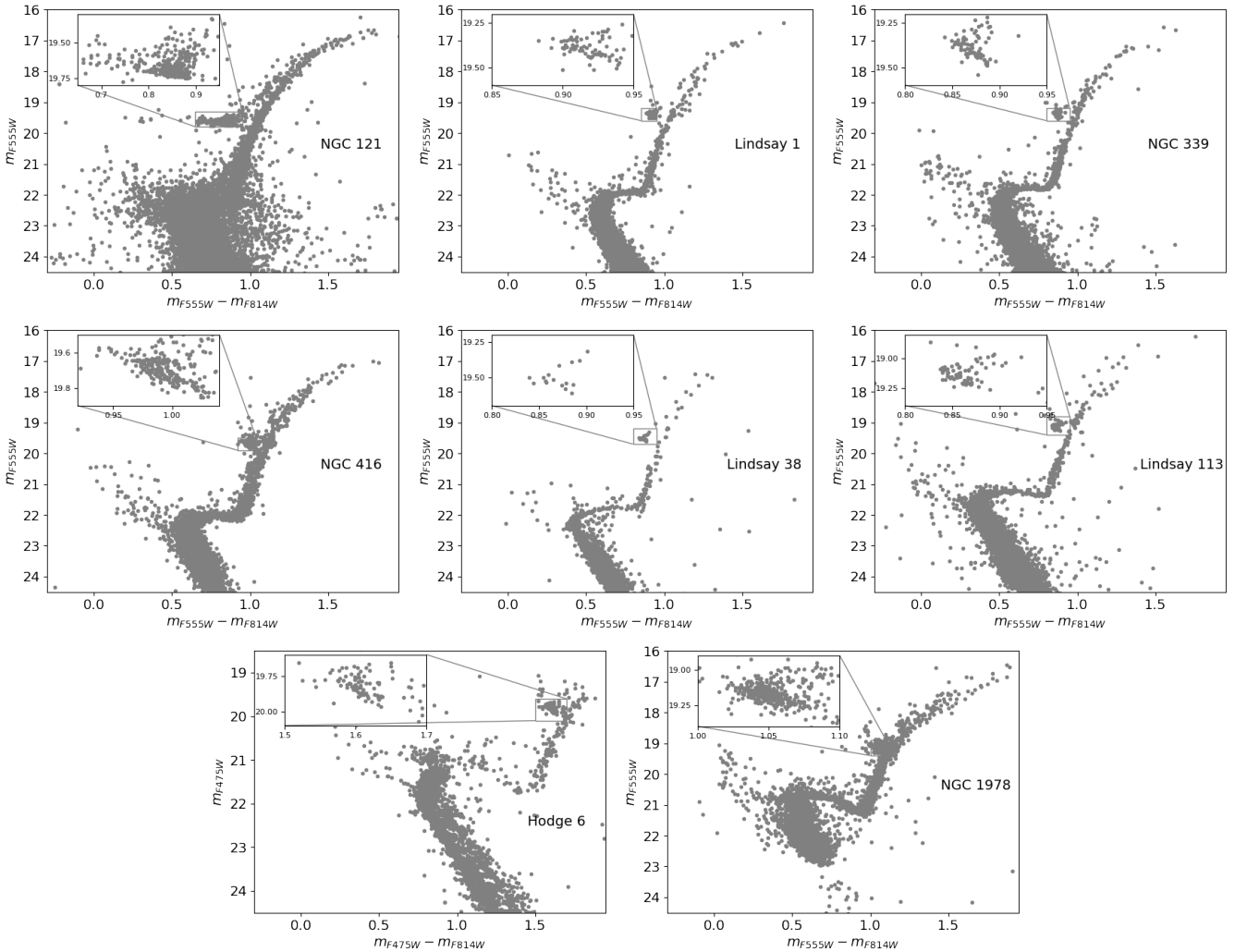


**Figure 1.** CMDs of NGC 121, Lindsay 1, NGC 339, NGC 416, Lindsay 38, Lindsay 113, Hodge 6 and NGC 1978 with a zoom on the HB/RC region. Except for Hodge 6, whose CMD is displayed in the F475W vs (F475W-F814W) diagram, all the other CMDs are F555W vs (F555W-F814W).

cluster works as follows. For any given cluster we apply to the models distance modulus and reddening values listed in Table 1, using the extinction coefficient for the *ACS* and *WFC3* filters from Goudfrooij et al. (2009, 2014). We then adjust  $E(B - V)$  to fit the cluster RGB with the track of the HB progenitor, and fix  $\eta_R$  to match the reddest part of the observed HB with models calculated with the minimum value of  $Y$ . We then vary the maximum value of  $Y$  at fixed  $\eta_R$  – or  $\eta_R$  and fixed initial  $Y$  – to reproduce by eye the slope and full colour extension of the HB. Due to the strong sensitivity of the HB morphology to variations of  $Y$  (and  $\eta_R$ ), we found with numerical tests that a simple fit by eye can give an accuracy on  $\Delta Y$  better than 0.01 (see Sect. 4).

We do not try to enforce the constraint of statistical agreement between the theoretical and observed star counts, because a perfect fit of star counts rests on the precise knowledge of, for example, the initial  $Y$  distribution among the cluster stars, that could be extremely complicated and/or discontinuous. The morphological constraints imposed on the matching synthetic HB are however sufficient to put strong bounds on  $\Delta Y$ , the maximum He abundance range, that is the main parameter discussed in this work. Obviously, our technique does not determine the exact number distribution of HB stars as a function of their initial  $Y$ .

Figure 2 shows the case of two clusters, one (Lindsay 1) representative of intermediate-age and old clusters (initial mass of He-normal HB progenitors lower than  $\sim 1.5 M_\odot$ ), and one (NGC 1978) representative of younger clusters but still populated by RGB stars with electron degenerate cores. For the sake of clarity we display selected HB evolutionary tracks without photometric errors applied. The tracks shown do not represent the best fit models for these two clusters that will then be presented in Sect. 4, rather their purpose is just to highlight trends in the CMD.

In both cases a variation  $\Delta Y$  at fixed  $\eta_R$  (and age) moves the HB tracks in an orthogonal direction with respect to the effect of varying  $\eta_R$  ( $\Delta\eta_R$ ) at fixed  $Y$  (see also Fig. 1 in Salaris et al. 2016), although the directions of the  $\Delta Y$  and  $\Delta\eta_R$  vectors change between the two age regimes. It is quite obvious even from this simple qualitative test shown in Fig. 2, that Lindsay 1 HB morphology can be matched only with  $\Delta Y > 0$ . On the other hand, the HB morphology of NGC 1978 seems more likely to be shaped by a range of  $\eta_R$ . We will see that the inclusion of photometric errors makes however difficult to draw firm conclusions for this cluster and the similar cluster Hodge 6.

We conclude this section with a test of our synthetic HB modelling on the well studied Galactic GC NGC 104 (total mass equal to  $\sim 7.8 \times 10^5 M_\odot$ , age  $\sim 12$  Gyr,  $[\text{Fe}/\text{H}] = -0.72$ , as summarized in Table 1) and compare with the synthetic HB modelling by Salaris et al. (2016), who found that a helium range  $\Delta Y = 0.03$  is needed to reproduce the observed HB morphology. Their result is in good agreement with several previous studies (Anderson et al. 2009; di Criscienzo et al. 2010; Milone et al. 2012; Gratton et al. 2013) who determined  $\Delta Y \sim 0.02\text{--}0.03$  for this GC.

We employed the same data (*BVI* photometry by Bergbusch & Stetson 2009) used by Salaris et al. (2016), an apparent distance modulus  $(m - M)_V = 13.37$  and reddening  $E(B - V) = 0.04$  (Harris 1996, 2010 edition), and calculated  $\alpha$ -enhanced stellar models for  $[\text{Fe}/\text{H}] = -0.72$ ,  $[\alpha/\text{Fe}] = +0.2$ , an age of 12 Gyr and various initial  $Y$  and  $\eta_R$ . We use here for the extinction  $A_B/A_V = 1.29719$  and  $A_I/A_V = 0.60329$ . Following the procedure described before, we find  $\eta_R = 0.34$  ( $\Delta M_{\text{RGB}} \sim 0.17 M_\odot$ ) and  $\Delta Y = 0.03$  from the match of the observed HB. Figure 3 compares the observed HB with synthetic HBs calculated with  $\eta_R = 0.34$  and both  $\Delta Y = 0$  (left-hand panel) and  $\Delta Y = 0.03$  (right-hand panel). A  $\Delta Y$  of only 0.025 pro-

duces a HB too short and  $\Delta Y = 0.035$  produces a HB slightly too extended compared to the observations,

Our derived  $\Delta Y = 0.03 \pm 0.005$  is in good agreement with what is found in the literature.

## 4 ANALYSIS OF THE MAGELLANIC CLOUDS' CLUSTER SAMPLE

### 4.1 NGC 121

NGC 121 (SMC) has been investigated by Dalessandro et al. (2016) and Niederhofer et al. (2017a). The latter found two distinct populations from the analysis of the RGB with appropriate filter combinations, and they also concluded that a He abundance spread  $\Delta Y = 0.025 \pm 0.005$  is needed to explain the morphology of the cluster HB. Therefore this cluster, with properties very similar to massive Milky Way GCs (total mass  $\sim 5.8 \times 10^5 M_\odot$ , age equal to  $\sim 10.5$  Gyr, and  $[\text{Fe}/\text{H}] = -1.30$ ), allows us to compare again our results with previous independent results. We found that  $\eta_R = 0.33$  (corresponding to a total RGB mass loss  $\Delta M_{\text{RGB}} \sim 0.145 M_\odot$ , irrespective of the initial  $Y$  of the models) and  $\Delta Y \sim 0.03$  are required to match the colour extension and slope of the observed HB, as shown in Fig. 4. A variation of  $\eta_R$  at constant initial  $Y$  would extend the synthetic HB orthogonally compared to the observations (see Fig. 2). The derived  $\Delta Y$  is consistent with Niederhofer et al. (2017a) result, based on a different set of HB stellar evolution models.

In the same Fig. 4 we display the effect of changing  $\Delta Y$  of the synthetic HBs by  $\pm 0.01$  around  $\Delta Y = 0.03$ . It is obvious that in this case the colour extension of the observed HB is clearly not matched by the synthetic stars, implying that the error on our estimates of  $\Delta Y$  is lower than 0.01. This is the typical upper limit to the error in the  $\Delta Y$  values obtained for the other clusters in our sample.

### 4.2 Lindsay 1

Lindsay 1 (SMC), has a mass and metallicity typical of a Galactic GC ( $1.7 \times 10^5 M_\odot$ ,  $[\text{Fe}/\text{H}] = -1.14$  respectively) but a younger age ( $\sim 7.5$  Gyr). Hollyhead et al. (2017) found a significant nitrogen abundance spread ( $\Delta[\text{N}/\text{Fe}] > 1$  dex) among stars located below the RGB bump, a signature of GC-like multiple stellar populations. Later, Niederhofer et al. (2017b) detected a photometric split of the RGB in suitable photometric filter combinations, a signature of a N spread among its stars.

We determine from our HB fitting procedure  $\eta_R = 0.3$  ( $\Delta M_{\text{RGB}} \sim 0.11 M_\odot$ ) and  $\Delta Y \sim 0.03$  (see Fig. 5).

### 4.3 NGC 339

NGC 339 is a SMC cluster with total mass equal to  $2.9 \times 10^5 M_\odot$ , an age of  $\sim 6$  Gyr, and  $[\text{Fe}/\text{H}] = -1.12$ . Niederhofer et al. (2017b) found a photometric RGB splitting, characteristic of the presence of the multiple stellar populations. From the HB fitting we determine  $\eta_R = 0.4$  ( $\Delta M_{\text{RGB}} \sim 0.14 M_\odot$ ) and  $\Delta Y \sim 0.03$  (see Fig. 5).

### 4.4 NGC 416

NGC 416 is a SMC cluster very similar to NGC 339, with a total mass equal to  $2.3 \times 10^5 M_\odot$ , an age  $\sim 6$  Gyr, and  $[\text{Fe}/\text{H}] = -1.00$ . We use here the data from Niederhofer et al. (2017b) corrected for differential reddening, that affects this cluster. Niederhofer et al.



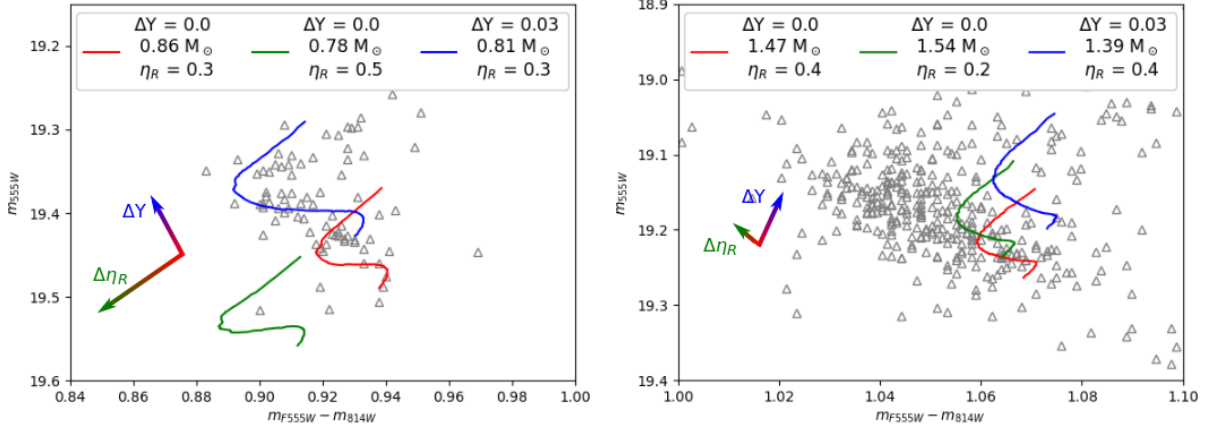


**Figure 2.** *Left:* HB of Lindsay 1 in grey open triangles. The HB stellar evolution tracks with initial main sequence mass  $M_{ini} = 0.97 M_{\odot}$ ,  $[Fe/H] = -1.14$ ,  $\Delta Y = 0$  (cluster age  $\sim 7.5$  Gyr) and  $\eta_R = 0.3$  and  $0.5$  are displayed with red and green lines, respectively. The track with initial main sequence mass  $M_{ini} = 0.92 M_{\odot}$ ,  $[Fe/H] = -1.14$ ,  $\Delta Y = 0.03$  (HB age  $\sim 7.5$  Gyr),  $\eta_R = 0.3$  is displayed with a blue line. The values of the corresponding current HB masses are displayed in the labels. *Right:* Horizontal branch of NGC 1978 in grey open triangles. HB tracks with initial mass  $M_{ini} = 1.60 M_{\odot}$ ,  $[Fe/H] = -0.35$ ,  $\Delta Y = 0$  (cluster age  $\sim 1.9$  Gyr),  $\eta_R = 0.4$  and  $0.2$  are displayed with red and green lines respectively. Tracks with an initial mass  $M_{ini} = 1.51 M_{\odot}$ ,  $[Fe/H] = -0.35$  and  $\Delta Y = 0.03$  (HB age  $\sim 1.9$  Gyr) and  $\eta_R = 0.4$  is displayed with a blue line. The current masses are displayed in the label.

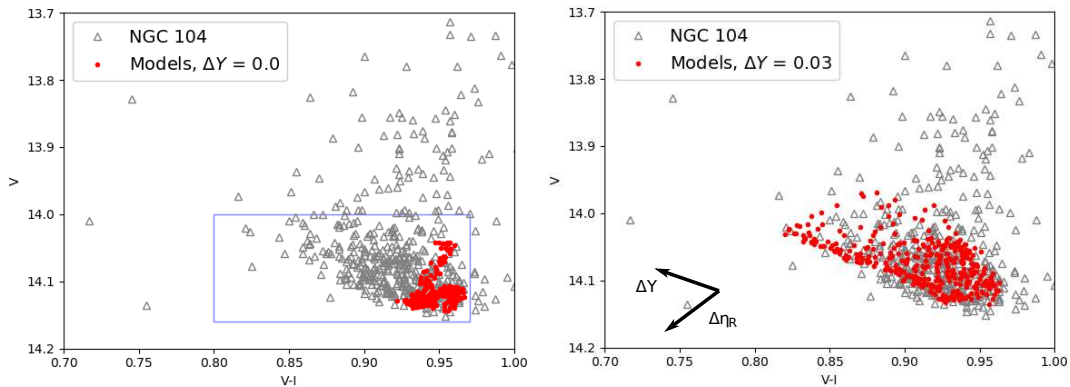


**Figure 3.** *VI* CMD of NGC 104 HB (grey open triangles) together with our synthetic HB models (red circles). *Left:* synthetic HB with  $\Delta Y=0$ . *Right:* Synthetic HB with  $\Delta Y=0.03$  and uniform helium abundance distribution. The number of synthetic and observed stars in the box (blue) delimiting the HB region is the same. The arrows describe the direction along which variations in  $Y$  and mass-loss work, the amplitude being arbitrary here.

(2017b) found also in this cluster a RGB splitting, signature of the presence of multiple stellar populations.

Our HB fitting provides  $\eta_R = 0.4$  ( $\Delta M_{RGB} \sim 0.145 M_{\odot}$ ) and  $\Delta Y = 0.065$  (see Fig. 6). This range of initial  $Y$  is much larger than in the previous clusters, and might be at least slightly overestimated if there is some residual differential reddening not accounted for, given that the reddening vector is aligned with the HB slope.

#### 4.5 Lindsay 38

The SMC cluster Lindsay 38 has an age similar to NGC 416 and NGC 339 ( $\sim 6$  Gyr), a lower mass ( $\sim 3.35 \times 10^4 M_{\odot}$ ) and a lower metallicity ( $[Fe/H] = -1.50$ ). The HB fitting provides  $\eta_R = 0.3$  ( $\Delta M_{RGB} \sim 0.09 M_{\odot}$ ), but there is no strong indication of  $\Delta Y > 0$ . Fig. 6 shows that  $\Delta Y=0.005$  is probably an upper limit to the range of initial He in this cluster.

#### 4.6 Lindsay 113

Lindsay 113 is the youngest SMC cluster in our sample ( $\sim 4.5$  Gyr), the least massive one ( $\sim 2.3 \times 10^4 M_{\odot}$ ), and metal-poor ( $[Fe/H] = -1.40$ ). We derive from the HB fitting  $\eta_R = 0.3$  ( $\Delta M_{RGB} \sim 0.08 M_{\odot}$ ), and again no strong signature of a helium abundance spread. Figure 6 shows that  $\Delta Y \sim 0.01$  is very likely an upper limit to the possible  $Y$  spread amongst the cluster stars.

#### 4.7 Hodge 6 and NGC 1978

These two LMC clusters are the youngest clusters in our sample, with ages equal to  $\sim 2.25$  (Hodge 6) and  $\sim 1.9$  Gyr (NGC 1978), and  $[Fe/H]$  around  $-0.40$  (see Table 1). Multiple populations have been found in both clusters (Martocchia et al. 2018b, Hollyhead et al. submitted).

Due to their younger age, the direction of the  $\Delta \eta_R$  and  $\Delta Y$  vectors is different compared to the case of the other clusters, as shown in Fig. 2. The different direction of these two vectors compared to the older clusters, coupled to the photometric error of these obser-

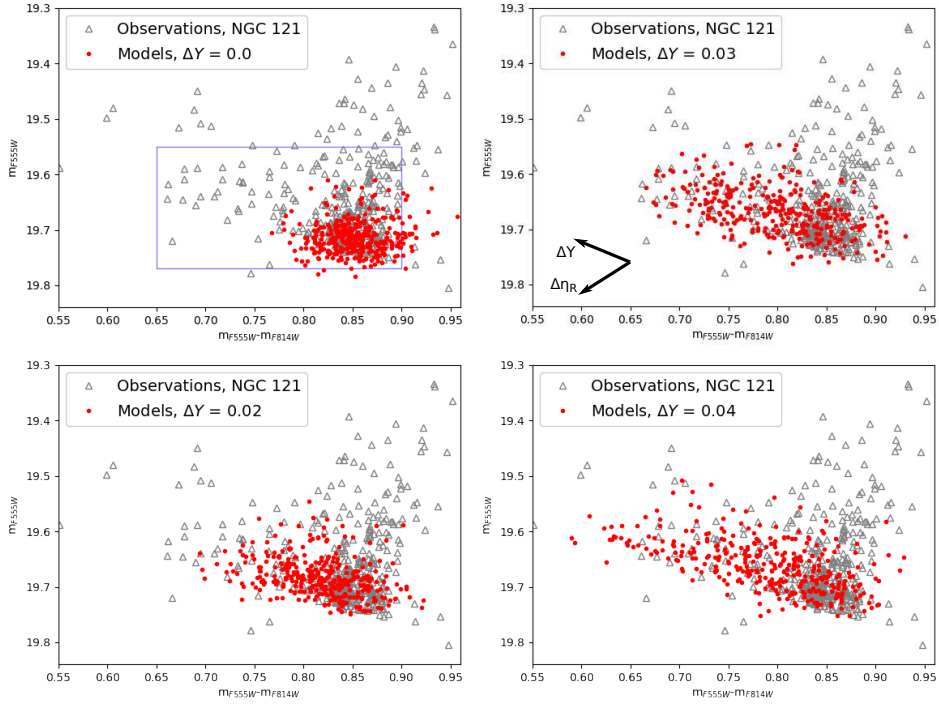


**Figure 4.** CMD of NGC 121 HB. Observations are represented by grey open triangles. Our synthetic HB models are overplotted in red. **Top panels:** Synthetic HB calculated with  $\Delta Y=0.0$  and  $\Delta Y=0.03$ , respectively, both assuming  $\eta_R = 0.33$ . The arrows describe the direction along which variations in  $Y$  and mass-loss work, the amplitude being arbitrary here. **Bottom panels:** Synthetic HBs with  $\eta_R = 0.33$  calculated with  $\Delta Y=0.02$  and  $\Delta Y=0.04$  (see text for details).

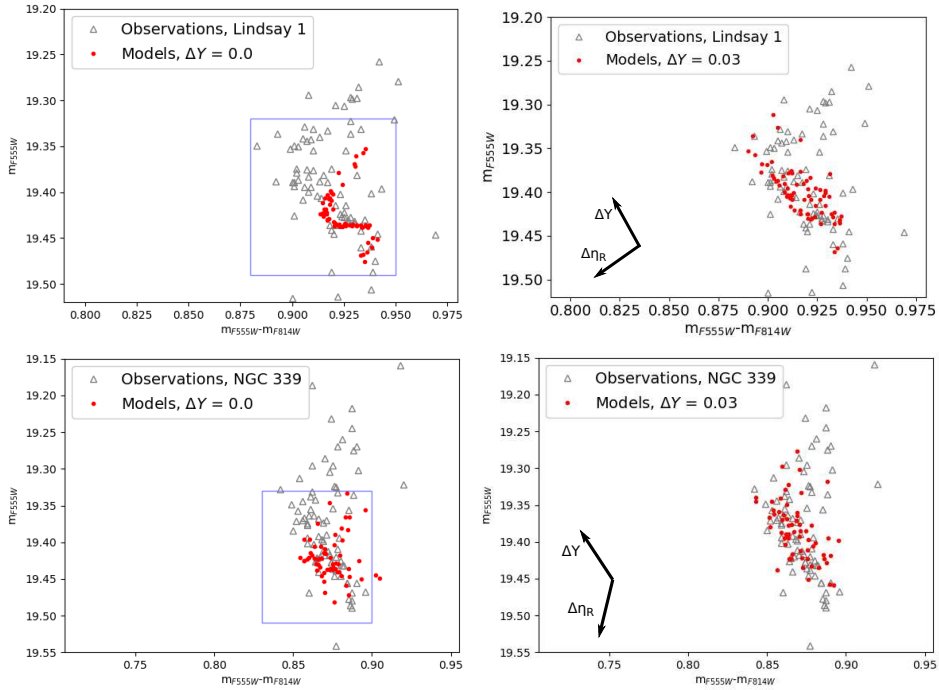


**Figure 5.** CMDs of Lindsay 1, and NGC 339 HBs. Observations are represented by grey open triangles. Our synthetic HB models are overplotted in red. **From left to right:** synthetic HB models at constant  $Y$  and best fit  $\eta_R$ , and models with both best fit  $\Delta Y$  and  $\eta_R$ , respectively. The arrows describe the direction along which variations in  $Y$  and mass-loss work, the amplitude being arbitrary here.

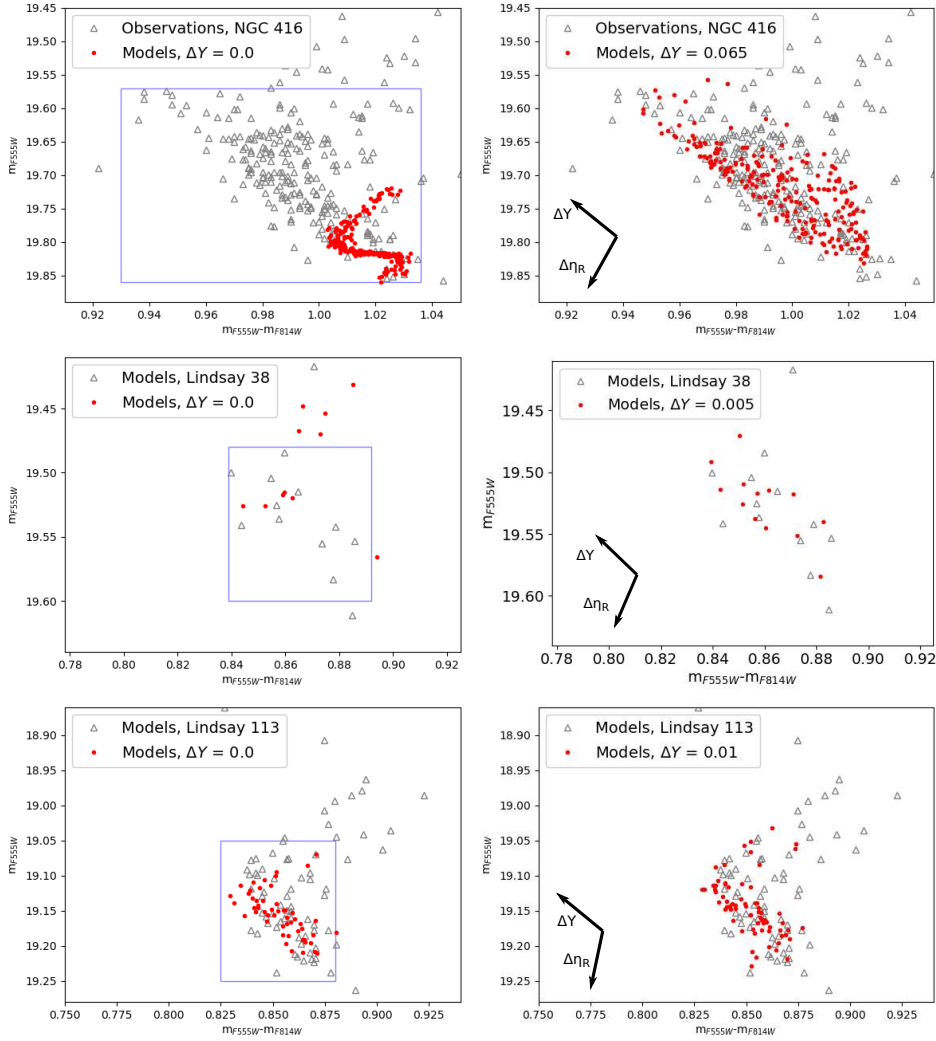


**Figure 6.** As Fig. 5 but for NGC 416, Lindsay 38 and Lindsay 113. The arrows describe the direction along which variations in  $Y$  and mass-loss work, the amplitude being arbitrary here.

variations – of the order of 0.01–0.03 mag in magnitudes and colours – makes it difficult to reach a definitive conclusion about the existence of a  $\Delta Y > 0$  in these two clusters. Figure. 7 shows that an initial He spread (at fixed mass loss) or a mass loss spread (at fixed  $Y$ ) can similarly approximate the colour extension and slope of the observed CMD of core He burning stars.

If we make the assumption that  $\eta_R$  must be constant, in agreement with the results for the other clusters in our sample, we would obtain  $\Delta Y \sim 0.06$  for Hodge 6, and  $\Delta Y \sim 0.04$  for NGC 1978. But without this assumption, the CMD analysis does not discriminate between a spread in  $\eta_R$  or in  $Y$  for these two clusters. However, we also note that Hodge 6 has the largest photometric errors of any of the clusters in our sample, adding further uncertainty for this cluster.

## 5 DISCUSSION

We have determined the total initial He abundance spread  $\Delta Y$  in a sample of intermediate-age, massive LMC and SMC clusters – and the old cluster NGC 121 – by reproducing the shape and colour extension of their HB/RC stars with synthetic HB models. Our de-

termined  $\Delta Y$  values are shown in Table 2. The typical error on these estimates of  $\Delta Y$  is below 0.01.

We can compare our results with the estimates by Lagioia et al. (2019). These authors found spreads of initial He abundances equal to  $0.009 \pm 0.006$ ,  $0.007 \pm 0.004$ ,  $0.010 \pm 0.003$ ,  $0.000 \pm 0.004$  for NGC 121, NGC 339, NGC 416 and Lindsay 1, respectively. These values are clearly smaller than our results in Table 2. But as mentioned already in the Introduction, the method employed by Lagioia et al. (2019) most likely determines mean abundance spreads among the cluster subpopulations, whereas our modelling tends to determine the maximum abundance spread, irrespective of the exact distribution of initial He abundances. This is quite clear by looking at the HB of NGC 121 in Fig. 4. The bulk of the HB population has  $(m_{F555W} - m_{F814W}) > 0.8$ , consistent with a negligible  $\Delta Y$  with just a plume of stars extending towards bluer colors and brighter magnitudes, that is, with significantly different initial  $Y$ .

The values in Table 2 are also plotted in Fig. 8 as a function of the mass of the host cluster. In the same figure we display also the maximum initial  $Y$  spread determined for a sample of Galactic GCs by Milone et al. (2018). Milone et al. (2018) found a trend between  $\Delta Y$  and the mass of the host cluster, that is clearly visible in Fig. 8

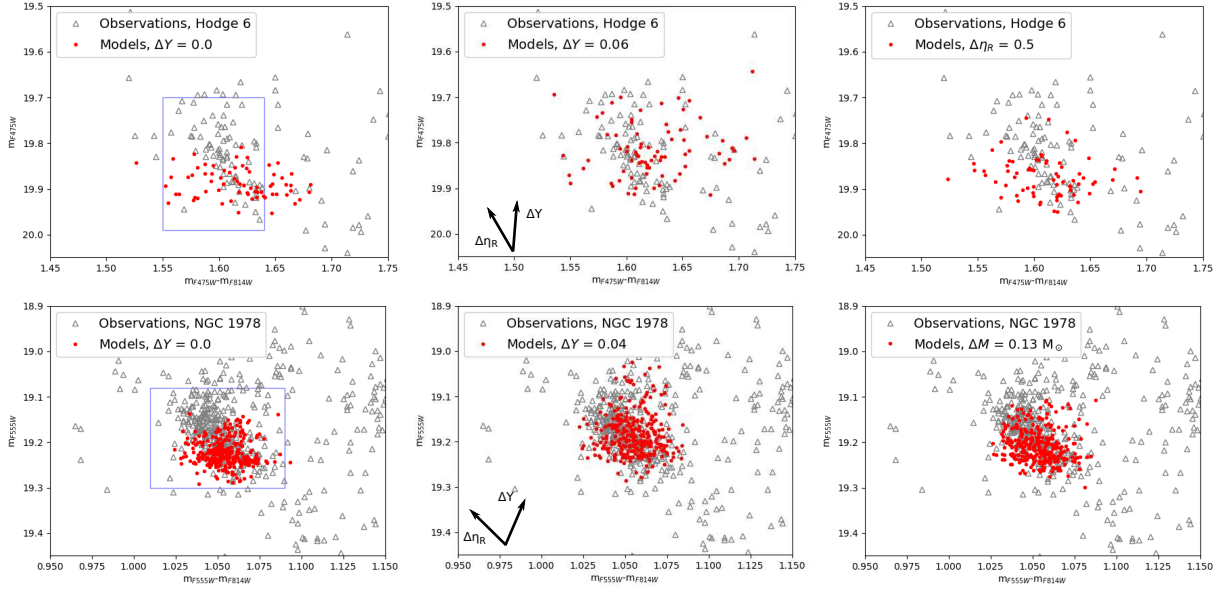


**Figure 7.** CMDs of Hodge 6 and NGC 1978, the two youngest clusters in our sample. Observations are denoted with grey open triangles, synthetic HB models are overlotted in red. *From left to right:*  $\Delta Y=0$  models, models with  $\Delta Y > 0$  ( $\eta_R$  fixed to the best fit value used in the left panel), and with  $\Delta\eta_R > 0$  ( $Y$  fixed to the He-normal value of the left panel). The arrows describe the direction along which variations in  $Y$  and mass-loss work, the amplitude being arbitrary here.

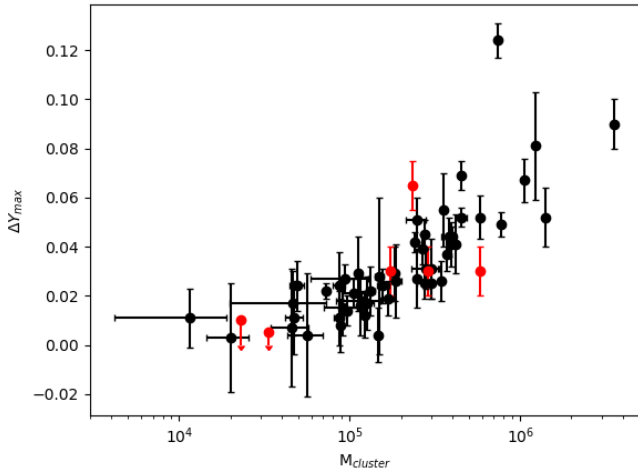


**Figure 8.** Relation between  $\Delta Y$  and cluster mass (in solar mass units). Galactic GC data from Milone et al. (2018) and Baumgardt & Hilker (2018) are displayed in black circles, the results for our SMC and LMC clusters are displayed as red circles.

and the results for our clusters follow this trend well. We found a Spearman rank-order correlation coefficient of 0.64 (p-value  $\sim 0.17$ ) between  $\Delta Y_{max}$  and the logarithm of the cluster mass. This result confirms the ubiquity of multiple stellar populations in massive intermediate-age clusters and GCs, questioning at the same time the distinction between these two classes of stellar systems. Interestingly, our very tentative determination of  $\Delta Y$  for NGC 1978 would fit the trend of Galactic GCs, whereas the  $\Delta Y$  for Hodge 6 would be much higher for its value of total mass (but note that this final measurement is highly uncertain due to the photometric errors and age of the cluster as discussed in Sec. 4.7).

We also searched for possible trends of  $\Delta Y$  with the cluster

ID	$\Delta Y_{max}$
NGC 121	0.03
Lindsay 1	0.03
NGC 339	0.03
NGC 416	0.065
Lindsay 38	$\leq 0.005$
Lindsay 113	$\leq 0.01$
Hodge 6	(0.06)
NGC 1978	(0.04)

**Table 2.** Initial helium abundance spread derived from the HB fitting. The values in parenthesis are determined in the assumption that the RGB mass loss does not vary among clusters' stars, because of a degeneracy between the effects of mass loss spread and He spread in these clusters (see text for details).

age amongst our cluster sample, but we did not find any statistically significant correlation (Spearman rank-order correlation coefficient of 0.35, p-value  $\sim 0.49$ , between  $\Delta Y_{max}$  and  $M_{cluster}$ ). This result is, to some degree, surprising given that the N abundance spreads has been found correlated with age in MCs intermediate-age clusters (Martocchia et al. 2018a,b), and may potentially shine a new light on the MP phenomenon.

## ACKNOWLEDGEMENTS

We warmly thank E. Dalessandro for useful discussions. W. Chantereau acknowledges funding from the Swiss National Science Foundation under grant P2GEP2\_171971. N.B. and W.C. gratefully acknowledge financial support from the European Research Council (ERC-CoG-646928, Multi-Pop). N.B. gratefully acknowledges financial support from the Royal Society (University Research Fellowship). Finally, we warmly thank the referee for the



pertinent suggestions that have helped us improve the presentation of our results.

## References

- Anderson J., Piotto G., King I. R., Bedin L. R., Guhathakurta P., 2009, *ApJ*, **697**, L58
- Asplund M., Grevesse N., Sauval A. J., Scott P., 2009, *ARA&A*, **47**, 481
- Bastian N., Lardo C., 2018, *ARA&A*, **56**, 83
- Baumgardt H., Hilker M., 2018, *MNRAS*, **478**, 1520
- Bergbusch P. A., Stetson P. B., 2009, *AJ*, **138**, 1455
- Busso G., et al., 2007, *A&A*, **474**, 105
- Caloi V., D'Antona F., 2007, *A&A*, **463**, 949
- Carretta E., Bragaglia A., Gratton R. G., Recio-Blanco A., Lucatello S., D'Orazi V., Cassisi S., 2010, *A&A*, **516**, A55
- Choi J., Dotter A., Conroy C., Cantiello M., Paxton B., Johnson B. D., 2016, *ApJ*, **823**, 102
- Coc A., Vangioni-Flam E., Descouvemont P., Adahchour A., Angulo C., 2004, *ApJ*, **600**, 544
- Dalessandro E., Salaris M., Ferraro F. R., Cassisi S., Lanzoni B., Rood R. T., Fusi Pecci F., Sabbi E., 2011, *MNRAS*, **410**, 694
- Dalessandro E., Salaris M., Ferraro F. R., Mucciarelli A., Cassisi S., 2013, *MNRAS*, **430**, 459
- Dalessandro E., Lapenna E., Mucciarelli A., Origlia L., Ferraro F. R., Lanzoni B., 2016, *ApJ*, **829**, 77
- Di Criscienzo M., Tailo M., Milone A. P., D'Antona F., Ventura P., Dotter A., Brocato E., 2015, *MNRAS*, **446**, 1469
- Glatt K., et al., 2008a, *AJ*, **135**, 1106
- Glatt K., et al., 2008b, *AJ*, **136**, 1703
- Glatt K., et al., 2011, *AJ*, **142**, 36
- Goudfrooij P., Puzia T. H., Kozhurina-Platais V., Chandar R., 2009, *AJ*, **137**, 4988
- Goudfrooij P., et al., 2014, *ApJ*, **797**, 35
- Gratton R. G., et al., 2013, *A&A*, **549**, A41
- Harris W. E., 1996, *AJ*, **112**, 1487
- Hollyhead K., et al., 2017, *MNRAS*, **465**, L39
- Hui-Bon-Hoa A., LeBlanc F., Hauschildt P. H., 2000, *ApJ*, **535**, L43
- Lagarde N., Decressin T., Charbonnel C., Eggenberger P., Ekström S., Palacios A., 2012, *A&A*, **543**, A108
- Lagioia E. P., Milone A. P., Marino A. F., Dotter A., 2019, *ApJ*, **871**, 140
- Martocchia S., et al., 2018a, *MNRAS*, **473**, 2688
- Martocchia S., et al., 2018b, *MNRAS*, **477**, 4696
- McDonald I., Zijlstra A. A., 2015, *MNRAS*, **448**, 502
- Michaud G., Richer J., Richard O., 2011, *A&A*, **529**, A60
- Milone A. P., et al., 2012, *ApJ*, **744**, 58
- Milone A. P., et al., 2018, *MNRAS*, **481**, 5098
- Mucciarelli A., Ferraro F. R., Origlia L., Fusi Pecci F., 2007, *AJ*, **133**, 2053
- Niederhofer F., et al., 2017a, *MNRAS*, **464**, 94
- Niederhofer F., et al., 2017b, *MNRAS*, **465**, 4159
- Piatti A. E., Keller S. C., Mackey A. D., Da Costa G. S., 2014, *MNRAS*, **444**, 1425
- Reimers D., 1975, *Memoires of the Societe Royale des Sciences de Liege*, **8**, 369
- Salaris M., Weiss A., Ferguson J. W., Fusilier D. J., 2006, *ApJ*, **645**, 1131
- Salaris M., Cassisi S., Pietrinferni A., 2016, *A&A*, **590**, A64
- Sbordone L., Salaris M., Weiss A., Cassisi S., 2011, *A&A*, **534**, A9
- Westerlund B. E., 1997, *The Magellanic Clouds*
- Yong D., Grundahl F., Norris J. E., 2015, *MNRAS*, **446**, 3319
- di Criscienzo M., Ventura P., D'Antona F., Milone A., Piotto G., 2010, *MNRAS*, **408**, 999
- di Criscienzo M., et al., 2011, *MNRAS*, **414**, 3381